

Solving Vlasov Equations Using NRxx Method

Zhenning Cai*, Ruo Li[†] and Yanli Wang[‡]

March 13, 2018

Abstract

In this paper, we propose a moment method to numerically solve the Vlasov equations using the framework of the NRxx method developed in [6, 8, 7] for the Boltzmann equation. Due to the same convection term of the Boltzmann equation and the Vlasov equation, it is very convenient to use the moment expansion in the NRxx method to approximate the distribution function in the Vlasov equations. The moment closure recently presented in [5] is applied to achieve the globally hyperbolicity so that the local well-posedness of the moment system is attained. This makes our simulations using high order moment expansion accessible in the case of the distribution far away from the equilibrium which appears very often in the solution of the Vlasov equations. With the moment expansion of the distribution function, the acceleration in the velocity space results in an ordinary differential system of the macroscopic velocity, thus is easy to be handled. The numerical method we developed can keep both the mass and the momentum conserved. We carry out the simulations of both the Vlasov-Poisson equations and the Vlasov-Poisson-BGK equations to study the linear Landau damping. The numerical convergence is exhibited in terms of the moment number and the spatial grid size, respectively. The variation of discretized energy as well as the dependence of the recurrence time on moment order is investigated. The linear Landau damping is well captured for different wave numbers and collision frequencies. We find that the Landau damping rate linearly and monotonically converges in the spatial grid size. The results are in perfect agreement with the theoretic data in the collisionless case.

Keywords: Vlasov equations; NRxx method; Landau damping

1 Introduction

The Vlasov equation is a differential equation describing the time evolution of the distribution function of plasma consisting of charged particles with the long-range (for example, Coulomb) interaction. The equation was first suggested for the description of plasma by A. Vlasov in 1938 [16]. Due to the presence of long-range Coulomb interaction in the plasma, Vlasov started from the Vlasov equation, which is a collisionless Boltzmann equation, and used a self-consistent collective field created by the charged plasma particles to get the Vlasov-Maxwell equations [11]. The Vlasov-Poisson (V-P) equations are an

*School of Mathematical Sciences, Peking University, Beijing, China, email: caizn@pku.edu.cn.

[†]HEDPS & CAPT, LMAM & School of Mathematical Sciences, Peking University, Beijing, China, email: rli@math.pku.edu.cn.

[‡]CAPT, Beijing International Center for Mathematical Research, & School of Mathematical Sciences, Peking University, Beijing, China, email: wangyanliwyl@gmail.com.

approximation of the Vlasov-Maxwell equations in the nonrelativistic zero-magnetic field limit. The V-P equations are used to describe various phenomena in plasma, in particular Landau damping and the distributions in a double layer plasma. The Vlasov-Pission-BGK (V-B) equations are also studied with a collision term presented as the BGK term. They are the simplest kinetic equations which correctly describe the essential features of collective and dissipative (entropy-producing) particle interactions in semiconductor plasmas [1, 2, 17, 18].

Due to the complex phenomena in the plasma, numerical simulation plays an important role in the study of the Vlasov and related equations. There are several kinds of methods to solve the Vlasov equations. The finite element method was proposed in [19, 20], which can be used to handle complicated boundary problems but inconvenient to solve the high dimension equations [10]. Meanwhile, the particle-in-cell (PIC) method [3] which used a finite number of macro-particles to approximate the plasma is easy to be implemented, and the method to discretize the Vlasov equations on a mesh of phase space was introduced to remedy the problem in PIC that the inherent artificial discrete particle noise made the description inaccurate. The semi-Lagrangian method [15] and the cubic interpolated propagation method [12] were also used to solve the Vlasov equations. However, the first method destroyed the local characters due to the reconstruction and the second one was quite expensive for the storage of the distribution function and its derivatives. In [10], Filbet put forward a new method to deal with the force term, which made the scheme keep the mass and energy conserved. Recently, an approach based on the moment method has been proposed in [13], and therein the distribution function was expanded using the Hermite polynomials with a prescribed macroscopic velocity chosen as the expansion center and a prescribed thermal velocity as the scaling factor at different locations.

In the past years, a regularized moment method was developed in [6] to numerically solve the Boltzmann equation. This method adopts the Hermite polynomial expansion to approximate the distribution function, with the basis function shifted by the local macroscopic velocity and scaled by the square root of the local temperature. The approximated distribution function is used to directly solve the Boltzmann equation without the deduction of the moment system up to arbitrary order of moments. The method therein was further explored as the NRxx method [8, 7] by introducing the regularization term using asymptotic expansion in term of the mean free path. Recently, a new regularization method [5, 4] was derived with the guarantee that the regularized moment system is globally hyperbolic. Due to the locally well-posedness provided by the global hyperbolicity, it is eventually accessible that approximating the distribution function far away from the equilibrium distribution by the stable simulation using large number of moments. Inspired by this progress, we in this paper develop the NRxx method to study the Vlasov equations, which is similar to the Boltzmann equation in the convection term, while the distribution function is much farther away from the equilibrium state than the gas flows, due to the long-range Coulomb interactions.

Here we are focusing on the V-P and V-B equations. With the moment expansion in the Vlasov equations, the convection part is smoothly handled by the original NRxx method for the Boltzmann equation. We discretize the regularized term given in [4] directly using the central difference scheme. Our deduction shows that the electric potential brings us an acceleration on the macroscopic velocity, thus it is very convenient to be numerically integrated. Currently, the collision term under our consideration is the simple BGK model to avoid distraction. The approximated electric potential is obtained by a three-point central scheme, and the numerical method keeps both the mass and the mo-

momentum conserved. By the numerical resolution study, it is exhibited that our method is numerically converged by the comparison of Landau damping rates obtained using different spatial grid size and number of moments. With the increasing of the number of moments, the recurrence time is almost linearly related to the square root of the moment expansion order. The discretized energy of our method only varies slightly in comparison with the overall energy. Since the Landau damping rate is affected by the wave number and the collision frequency, different wave numbers and collision frequencies are extensively studied. The wave numbers ranging from 0.2 to 0.5 are simulated, and the collision frequencies are taken as 0.0 (the collisionless case), 0.01 and 0.05. The results show that our method can capture the linear Landau damping very well and the damping rates obtained is in quantitative agreement with the theoretic data. We find with surprise that the numerical Landau damping rate is linearly and monotonically converged in term of the spatial grid size. Particularly, the numerical damping rate converges to the theoretic data perfectly in the collisionless case. This observation inspires us to predict the Landau damping rates by the extrapolation of our numerical damping rates with presence of the collision term.

The layout of this paper is as follows: in Section 2, the regularized moment system is deduced for the Vlasov-BGK equations. In Section 3, we present the detailed procedure of the numerical method. In Section 4, the numerical examples including the numerical resolution study and the linear Landau damping simulation with different parameters are presented. Some concluding remarks are given in the last section.

2 Regularized Moment System

Let $f(t, \mathbf{x}, \mathbf{v})$, which depends on time t , position $\mathbf{x} \in \Omega \subset \mathbb{R}^3$ and the microscopic velocity $\mathbf{v} \in \mathbb{R}^3$, be the distribution function depicting the motion of particles. It is governed by the V-B equations

$$\frac{\partial f}{\partial t} + \mathbf{v} \cdot \nabla_{\mathbf{x}} f + \mathbf{F}(t, \mathbf{x}, \mathbf{v}) \cdot \nabla_{\mathbf{v}} f = \nu(f_M - f), \quad (2.1)$$

where $\nu(t, \mathbf{x})$ denotes the collision frequency, and $\mathbf{F}(t, \mathbf{x}, \mathbf{v})$ is the electric force produced by the self-consistent electric filed $\mathbf{E}(t, \mathbf{x})$:

$$\mathbf{F}(t, \mathbf{x}, \mathbf{v}) = \frac{q}{m} \mathbf{E}(t, \mathbf{x}), \quad \mathbf{E}(t, \mathbf{x}) = -\nabla_{\mathbf{x}} \phi(t, \mathbf{x}), \quad -\Delta_{\mathbf{x}} \phi = q \frac{\rho}{\epsilon_0}, \quad (2.2)$$

where $\phi(t, \mathbf{x})$ is the electric potential produced by the particles; ρ , q , m and ϵ_0 stand for the density, the single charge, the mass of one particle and the electric constant respectively; f_M is the Maxwellian defined as

$$f_M = \frac{\rho(t, \mathbf{x})}{(2\pi u_{th}(t, \mathbf{x}))^{3/2}} \exp\left(-\frac{|\mathbf{v} - \mathbf{u}(t, \mathbf{x})|^2}{2u_{th}(t, \mathbf{x})}\right), \quad (2.3)$$

where the parameter $u_{th}(t, \mathbf{x})$ is the thermal velocity [13], \mathbf{u} is the macroscopic velocity and $\rho(t, \mathbf{x})$ is the same as that in (2.2). f_M is related to f by

$$\int_{\mathbb{R}^3} f(\mathbf{v}) \begin{pmatrix} 1 \\ \mathbf{v} \\ |\mathbf{v}|^2 \end{pmatrix} d\mathbf{v} = \int_{\mathbb{R}^3} f_M(\mathbf{v}) \begin{pmatrix} 1 \\ \mathbf{v} \\ |\mathbf{v}|^2 \end{pmatrix} d\mathbf{v}. \quad (2.4)$$

In the case of $\nu = 0$, we get the V-P equations. The relations between the macroscopic variables and the distribution function are deduced as

$$\rho(t, \mathbf{x}) = \int_{\mathbb{R}^3} f(t, \mathbf{x}, \mathbf{v}) d\mathbf{v}, \quad (2.5)$$

$$\rho(t, \mathbf{x}) \mathbf{u}(t, \mathbf{x}) = \int_{\mathbb{R}^3} \mathbf{v} f(t, \mathbf{x}, \mathbf{v}) d\mathbf{v}, \quad (2.6)$$

$$\rho(t, \mathbf{x}) |\mathbf{u}(t, \mathbf{x})|^2 + 3\rho(t, \mathbf{x}) u_{th}(t, \mathbf{x}) = \int_{\mathbb{R}^3} |\mathbf{v}|^2 f(t, \mathbf{x}, \mathbf{v}) d\mathbf{v}. \quad (2.7)$$

The conservation of mass, momentum and total energy are all valid for the V-B and V-P equations. Multiplying the equation (2.1) by 1 and \mathbf{v} , direct integration with \mathbf{v} and \mathbf{x} gives us

$$\frac{d}{dt} \int_{\mathbb{R}^3 \times \mathbb{R}^3} f(t, \mathbf{x}, \mathbf{v}) d\mathbf{x} d\mathbf{v} = 0, \quad t \in \mathbb{R}^+, \quad (2.8)$$

$$\frac{d}{dt} \int_{\mathbb{R}^3 \times \mathbb{R}^3} \mathbf{v} f(t, \mathbf{x}, \mathbf{v}) d\mathbf{x} d\mathbf{v} = 0, \quad t \in \mathbb{R}^+. \quad (2.9)$$

Multiplying the equation (2.1) by $|\mathbf{v}|^2$ and integrating by parts, we get the conservation of the total energy for the system (2.1) and (2.2):

$$\frac{d}{dt} \left(\int_{\mathbb{R}^3 \times \mathbb{R}^3} f(t, \mathbf{x}, \mathbf{v}) |\mathbf{v}|^2 d\mathbf{x} d\mathbf{v} + \int_{\mathbb{R}^3} |\mathbf{E}(t, \mathbf{x})|^2 d\mathbf{x} \right) = 0, \quad t \in \mathbb{R}^+. \quad (2.10)$$

2.1 Hermite expansion of the distribution function

Following the method in [6, 9], we expand the distribution function into Hermite series as

$$f(\mathbf{v}) = \sum_{\alpha \in \mathbb{N}^3} f_\alpha \mathcal{H}_{u_{th}, \alpha}(\boldsymbol{\xi}), \quad (2.11)$$

where $\alpha = (\alpha_1, \alpha_2, \alpha_3)$ is a three-dimensional multi-index, and

$$\boldsymbol{\xi} = \frac{\mathbf{v} - \mathbf{u}}{\sqrt{u_{th}}}. \quad (2.12)$$

The basis functions $\mathcal{H}_{u_{th}, \alpha}$ are defined as

$$\mathcal{H}_{u_{th}, \alpha}(\boldsymbol{\xi}) = \prod_{d=1}^3 \frac{1}{\sqrt{2\pi}} u_{th}^{-\frac{\alpha_d+1}{2}} He_{\alpha_d}(\xi_d) \exp\left(-\frac{\xi_d^2}{2}\right), \quad (2.13)$$

where He_{α_d} is the Hermite polynomial

$$He_n(x) = (-1)^n \exp\left(\frac{x^2}{2}\right) \frac{d^n}{dx^n} \exp\left(-\frac{x^2}{2}\right). \quad (2.14)$$

For convenience, $He_n(x)$ is taken as zero if $n < 0$, thus $\mathcal{H}_{u_{th}, \alpha}(\boldsymbol{\xi})$ is zero when any component of α is negative. With such an expansion, the Maxwellian f_M can be written as

$$f_M(\mathbf{v}) = \rho \mathcal{H}_{u_{th}, 0}(\boldsymbol{\xi}), \quad (2.15)$$

and the BGK collision term is written as

$$\nu(f_M - f) = -\nu \sum_{|\alpha| \geq 1} f_\alpha \mathcal{H}_{u_{th}, \alpha}(\boldsymbol{\xi}). \quad (2.16)$$

The definition of $\boldsymbol{\xi}$ shows that each basis function is an exponentially decreasing function multiplied by a multi-dimensional Hermite polynomial shifted by the local macroscopic velocity \mathbf{u} and scaled by the square root of the local thermal velocity u_{th} . For any vector \mathbf{u}' and positive number u'_{th} , if the distribution function f is expanded as

$$f(\mathbf{v}) = \sum_{\alpha \in \mathbb{N}^3} f'_\alpha \mathcal{H}_{u'_{th}, \alpha}(\boldsymbol{\xi}'), \quad \boldsymbol{\xi}' = \frac{\mathbf{v} - \mathbf{u}'}{\sqrt{u'_{th}}}, \quad (2.17)$$

then the following relations hold

$$\rho = f'_0, \quad (2.18a)$$

$$\rho \mathbf{u} = \rho \mathbf{u}' + (f'_{e_d})_{d=1,2,3}^T, \quad (2.18b)$$

$$\rho |\mathbf{u}|^2 + 3\rho u_{th} = 2\rho \mathbf{u} \cdot \mathbf{u}' - \rho |\mathbf{u}'|^2 + \sum_{d=1}^3 (u'_{th} f'_0 + 2f'_{2e_d}). \quad (2.18c)$$

In the case of $\mathbf{u}' = \mathbf{u}$ and $u'_{th} = u_{th}$ in (2.18), the following relations between the coefficients f_α can be verified:

$$f_0 = \rho(t, \mathbf{x}), \quad f_{e_i} = 0, \quad \sum_{d=1}^3 f_{2e_d} = 0, \quad i = 1, 2, 3. \quad (2.19)$$

Moreover, direct calculations give us the relations between the coefficients f_α in (2.11) as

$$q_i = 2f_{3e_i} + \sum_{d=1}^3 f_{2e_d + e_i}, \quad (2.20)$$

$$p_{ij} - \frac{1}{3} \delta_{ij} \sum_{d=1}^3 p_{dd} = (1 + \delta_{ij}) f_{e_i + e_j}. \quad (2.21)$$

where $i, j = 1, 2, 3$, q_i and p_{ij} are related to f by

$$q_i = \frac{1}{2} \int_{\mathbb{R}^3} |\mathbf{v} - \mathbf{u}|^2 (v_i - u_i) f d\mathbf{v}, \quad (2.22)$$

$$p_{i,j} = \int_{\mathbb{R}^3} (v_i - u_i)(v_j - u_j) f d\mathbf{v}. \quad (2.23)$$

2.2 Moment expansion of Vlasov equation

To get the moment system, we substitute the expansion (2.11) into (2.1) and then match the coefficients for the same basis functions. Taking the temporal and spatial derivatives directly on the basis functions $\mathcal{H}_{u_{th}, \alpha}$, the term with the expansion (2.11)

$$\frac{\partial f}{\partial t} + \mathbf{v} \cdot \nabla_{\mathbf{x}} f$$

is expanded as

$$\begin{aligned}
& \sum_{\alpha \in \mathbb{N}^3} \left\{ \left(\frac{\partial f_\alpha}{\partial t} + \sum_{d=1}^3 \frac{\partial u_d}{\partial t} f_{\alpha - e_d} + \frac{1}{2} \frac{\partial u_{th}}{\partial t} \sum_{d=1}^3 f_{\alpha - 2e_d} \right) \right. \\
& + \sum_{j=1}^3 \left[\left(u_{th} \frac{\partial f_{\alpha - e_j}}{\partial x_j} + u_j \frac{\partial f_\alpha}{\partial x_j} + (\alpha_j + 1) \frac{\partial f_{\alpha + e_j}}{\partial x_j} \right) \right. \\
& + \sum_{d=1}^3 \frac{\partial u_d}{\partial x_j} (u_{th} f_{\alpha - e_d - e_j} + u_j f_{\alpha - e_d} + (\alpha_j + 1) f_{\alpha - e_d + e_j}) \\
& \left. \left. + \frac{1}{2} \frac{\partial u_{th}}{\partial x_j} \sum_{d=1}^3 (u_{th} f_{\alpha - 2e_d - e_j} + u_j f_{\alpha - 2e_d} + (\alpha_j + 1) f_{\alpha - 2e_d + e_j}) \right] \right\} \mathcal{H}_{u_{th}, \alpha} \left(\frac{\boldsymbol{\xi} - \mathbf{u}}{\sqrt{u_{th}}} \right), \tag{2.24}
\end{aligned}$$

the acceleration term $\mathbf{F} \cdot \nabla_{\mathbf{v}} f$ is expanded as

$$- \sum_{\alpha \in \mathbb{N}^3} \sum_{d=1}^3 F_d f_{\alpha - e_d} \mathcal{H}_{u_{th}, \alpha} \left(\frac{\boldsymbol{\xi} - \mathbf{u}}{\sqrt{u_{th}}} \right), \tag{2.25}$$

and the collision term $\nu(f_M - f)$ is expanded as

$$\nu \sum_{|\alpha| > 1} f_\alpha \mathcal{H}_{u_{th}, \alpha} \left(\frac{\boldsymbol{\xi} - \mathbf{u}}{\sqrt{u_{th}}} \right). \tag{2.26}$$

Substituting these expansions back into (2.1), and collecting coefficients for the same basis functions, we get the following general moment equations with a slight rearrangement:

$$\begin{aligned}
& \frac{\partial f_\alpha}{\partial t} + \sum_{d=1}^3 \left(\frac{\partial u_d}{\partial t} + \sum_{j=1}^3 u_j \frac{\partial u_d}{\partial x_j} - F_d \right) f_{\alpha - e_d} + \frac{1}{2} \left(\frac{\partial u_{th}}{\partial t} + \sum_{j=1}^3 u_j \frac{\partial u_{th}}{\partial x_j} \right) \sum_{d=1}^3 f_{\alpha - 2e_d} \\
& + \sum_{j,d=1}^3 \left[\frac{\partial u_d}{\partial x_j} (u_{th} f_{\alpha - e_d - e_j} + (\alpha_j + 1) f_{\alpha - e_d + e_j}) + \frac{1}{2} \frac{\partial u_{th}}{\partial x_j} (u_{th} f_{\alpha - 2e_d - e_j} + (\alpha_j + 1) f_{\alpha - 2e_d + e_j}) \right] \\
& + \sum_{j=1}^3 \left(u_{th} \frac{\partial f_{\alpha - e_j}}{\partial x_j} + u_j \frac{\partial f_\alpha}{\partial x_j} + (\alpha_j + 1) \frac{\partial f_{\alpha + e_j}}{\partial x_j} \right) = \nu(1 - \delta(\alpha)) f_\alpha, \tag{2.27}
\end{aligned}$$

where $\delta(\alpha)$ is defined by

$$\delta(\alpha) = \begin{cases} 0, & \text{if } |\alpha| \geq 2, \\ 1, & \text{otherwise.} \end{cases} \tag{2.28}$$

Following the method in [7], we deduce the mass conservation in the case of $\alpha = 0$ as

$$\frac{\partial f_0}{\partial x_j} + \sum_{j=1}^3 \left(u_j \frac{\partial f_0}{\partial x_j} + f_0 \frac{\partial u_j}{\partial x_j} \right) = 0. \tag{2.29}$$

If we set $\alpha = e_d$, with $d = 1, 2, 3$, (2.27) reduces to

$$f_0 \left(\frac{\partial u_d}{\partial t} + \sum_{j=1}^3 u_j \frac{\partial u_d}{\partial x_j} - F_d \right) + f_0 \frac{\partial u_{th}}{\partial x_d} + u_{th} \frac{\partial f_0}{\partial x_d} + \sum_{j=1}^3 (\delta_{jd} + 1) \frac{\partial f_{e_d + e_j}}{\partial x_j} = 0, \tag{2.30}$$

which is simplified as

$$f_0 \left(\frac{\partial u_d}{\partial t} + \sum_{j=1}^3 u_j \frac{\partial u_d}{\partial x_j} - F_d \right) + \sum_{j=1}^3 \frac{\partial p_{jd}}{\partial x_j} = 0. \quad (2.31)$$

Then we consider the case of $|\alpha| \geq 2$. Multiplying $|\mathbf{v} - \mathbf{u}|^2$ on both sides of (2.1), and integrating with respect to \mathbf{v} on \mathbb{R}^3 , we have

$$f_0 \left(\frac{\partial u_{th}}{\partial t} + \sum_{j=1}^3 u_j \frac{\partial u_{th}}{\partial x_j} \right) + \frac{2}{3} \sum_{j=1}^3 \left(\frac{\partial q_j}{\partial x_j} + \sum_{d=1}^3 p_{jd} \frac{\partial u_d}{\partial x_j} \right) = 0. \quad (2.32)$$

Remark 1. Since

$$\int_{\mathbb{R}^3} |\mathbf{v} - \mathbf{u}|^2 \frac{\partial f}{\partial v_i} d\mathbf{v} = -2 \int_{\mathbb{R}^3} (v_i - u_i) f d\mathbf{v} = 0, \quad i = 1, 2, 3, \quad (2.33)$$

the acceleration term does not appear in (2.32).

Substituting (2.31) and (2.32) into (2.27), we eliminate the temporal derivatives of \mathbf{v} and u_{th} . Then the quasi-linear form of the moment system reads:

$$\begin{aligned} \frac{\partial f_\alpha}{\partial t} - \frac{1}{f_0} \sum_{d=1}^3 \sum_{j=1}^3 \frac{\partial p_{jd}}{\partial x_j} f_{\alpha-e_d} - \frac{1}{3f_0} \sum_{j=1}^3 \left(\frac{\partial q_j}{\partial x_j} + \sum_{d=1}^3 p_{jd} \frac{\partial u_d}{\partial x_j} \right) \sum_{d=1}^3 f_{\alpha-2e_d} \\ + \sum_{j,d=1}^3 \left[\frac{\partial u_d}{\partial x_j} (u_{th} f_{\alpha-e_d-e_j} + (\alpha_j + 1) f_{\alpha-e_d+e_j}) + \frac{1}{2} \frac{\partial u_{th}}{\partial x_j} (u_{th} f_{\alpha-2e_d-e_j} + (\alpha_j + 1) f_{\alpha-2e_d+e_j}) \right] \\ + \sum_{j=1}^3 \left(u_{th} \frac{\partial f_{\alpha-e_j}}{\partial x_j} + u_j \frac{\partial f_\alpha}{\partial x_j} \right) + \sum_{j=1}^3 (\alpha_j + 1) \frac{\partial f_{\alpha+e_j}}{\partial x_j} = \nu(1 - \delta(\alpha)) f_\alpha, \quad \forall |\alpha| \geq 2. \end{aligned} \quad (2.34)$$

We collect the equations (2.29), (2.31), (2.32) and (2.34) together to obtain a moment system with infinite number of equations.

2.3 Closure of the moment system

With a truncation of (2.11), (2.34) will result in a finite moment system. Precisely, we let $M \geq 3$ be a positive integer and only the coefficients in the set $\mathcal{M} = \{f_\alpha\}_{|\alpha| \leq M}$ are considered. Let $F_M(\mathbf{u}, u_{th})$ denotes the linear space spanned by all $\mathcal{H}_{u_{th}, \alpha}(\boldsymbol{\xi})$'s with $|\alpha| \leq M$, and the expansion (2.11) is truncated as

$$f(\mathbf{v}) \approx \sum_{|\alpha| \leq M} f_\alpha \mathcal{H}_{u_{th}, \alpha} \left(\frac{\mathbf{v} - \mathbf{u}}{\sqrt{u_{th}}} \right), \quad (2.35)$$

with $f(\mathbf{v}) \in F_M(\mathbf{u}, u_{th})$ and $f_\alpha \in \mathcal{M}$. The moment equations which contain $\partial f_\alpha / \partial t$ with $|\alpha| > M$ are disregarded in (2.34). Then, (2.29), (2.31) and (2.34) with $2 \leq |\alpha| \leq M$ lead to a system with finite number of equations.

Due to the presence of the terms with $\partial f_{\alpha+e_j} / \partial x_j$, $|\alpha| = M$, the moment system we obtained is not closed yet. We rewrite (2.34) into the form below:

$$\frac{\partial f_\alpha}{\partial t} + \mathcal{A}_\alpha + \mathcal{B}_\alpha = \nu(1 - \delta(\alpha)) f_\alpha, \quad (2.36)$$

where in the case of $2 \leq |\alpha| < M$,

$$\begin{aligned}\mathcal{A}_\alpha &= -\frac{1}{f_0} \sum_{d=1}^3 \sum_{j=1}^3 \frac{\partial p_{jd}}{\partial x_j} f_{\alpha-e_d} + \cdots + \sum_{j=1}^3 \left(u_{th} \frac{\partial f_{\alpha-e_j}}{\partial x_j} + u_j \frac{\partial f_\alpha}{\partial x_j} \right) \\ &\quad + \sum_{j=1}^3 (\alpha_j + 1) \frac{\partial f_{\alpha+e_j}}{\partial x_j}, \\ \mathcal{B}_\alpha &= 0,\end{aligned}$$

and in the case of $|\alpha| = M$,

$$\begin{aligned}\mathcal{A}_\alpha &= -\frac{1}{f_0} \sum_{d=1}^3 \sum_{j=1}^3 \frac{\partial p_{jd}}{\partial x_j} f_{\alpha-e_d} + \cdots + \sum_{j=1}^3 \left(u_{th} \frac{\partial f_{\alpha-e_j}}{\partial x_j} + u_j \frac{\partial f_\alpha}{\partial x_j} \right), \\ \mathcal{B}_\alpha &= \sum_{j=1}^3 \mathcal{B}_{\alpha,j}, \quad \mathcal{B}_{\alpha,j} = (\alpha_j + 1) \frac{\partial f_{\alpha+e_j}}{\partial x_j}.\end{aligned}$$

Clearly, the moments $f_{\alpha+e_j}$ in term \mathcal{B}_α with $|\alpha| = M$ are not in the set of moments $\mathcal{M} = \{f_\alpha\}_{|\alpha| \leq M}$, and have to be substituted by some expressions consisting of lower order moments to make the moment system closed. If we simply let $\mathcal{B}_\alpha = 0$, the Grad-type system associated with the moment set $\mathcal{M} = \{f_\alpha\}_{|\alpha| \leq M}$ is obtained. It is known that the Grad-type system is not locally well-posed due to the lack of the global hyperbolicity, which results in numerical blow-up when the distribution function is far away from the equilibrium state. The regularization method in [4, 5] is adopted here to achieve a globally hyperbolic moment closure. The $(M+1)$ -st order terms are substituted as bellow

$$\frac{\partial f_{\alpha+e_j}}{\partial x_j} \longrightarrow - \left(\sum_{d=1}^3 f_{\alpha-e_d+e_j} \frac{\partial u_d}{\partial x_j} + \frac{1}{2} \left(\sum_{d=1}^D f_{\alpha-2e_d+e_j} \frac{\partial u_{th}}{\partial x_j} \right) \right), \quad |\alpha| = M, \quad j = 1, 2, 3. \quad (2.37)$$

Let $\hat{\mathcal{B}}_\alpha$ denote the regularization term based on the characteristic speed correction in [4, 5] for $|\alpha| = M$

$$\hat{\mathcal{B}}_\alpha = - \sum_{d=1}^3 \hat{\mathcal{B}}_{\alpha,j}, \quad \hat{\mathcal{B}}_{\alpha,j} = - \left(\sum_{d=1}^3 f_{\alpha-e_d+e_j} \frac{\partial u_d}{\partial x_j} + \frac{1}{2} \sum_{d=1}^D f_{\alpha-2e_d+e_j} \frac{\partial u_{th}}{\partial x_j} \right). \quad (2.38)$$

Substituting the $(M+1)$ -st order term \mathcal{B}_α with the regularization term $\hat{\mathcal{B}}_\alpha$, the moment equations are revised as

$$\frac{\partial f_\alpha}{\partial t} + \mathcal{A}_\alpha + \hat{\mathcal{B}}_\alpha = \nu(1 - \delta(\alpha))f_\alpha, \quad (2.39)$$

with $\hat{\mathcal{B}}_\alpha = \mathcal{B}_\alpha = 0$ for $2 \leq |\alpha| < M$. If the distribution function f only depends on x_1 in the spatial direction, we have that

$$\hat{\mathcal{B}}_{\alpha,j} = 0, \quad \text{for } j = 2, 3. \quad (2.40)$$

Remark 2. The regularized moment system (2.39) is not able to be written into a conservation law, for the presence of the regularization term. If we let $\hat{\mathcal{B}}_\alpha = 0$ with $|\alpha| = M$, the system changes into the conservative Grad-type system.

3 Numerical Method

The numerical scheme for the regularized moment system (2.39) is a natural extension of the method in [6]. By a standard fraction step method, we split the V-B equations into the following parts:

- the convection step:

$$\frac{\partial f}{\partial t} + \mathbf{v} \cdot \nabla_{\mathbf{x}} f = 0, \quad (3.1)$$

- the acceleration step:

$$\frac{\partial f}{\partial t} + \mathbf{F}(t, \mathbf{x}, \mathbf{v}) \cdot \nabla_{\mathbf{v}} f = 0, \quad (3.2)$$

$$\mathbf{F}(t, \mathbf{x}, \mathbf{v}) = \frac{q}{m} \mathbf{E}(t, \mathbf{x}), \quad \mathbf{E}(t, \mathbf{x}) = -\nabla_{\mathbf{x}} \phi(t, \mathbf{x}), \quad -\Delta_{\mathbf{x}} \phi = q \frac{\rho}{\epsilon_0}. \quad (3.3)$$

- the collision step:

$$\frac{\partial f}{\partial t} = \nu(f_M - f). \quad (3.4)$$

We observe that only (2.31) contains the electric force \mathbf{F} in the governing equations. Thus the governing equations of the acceleration part turn into

$$\partial_t \mathbf{u} = \mathbf{F}, \quad (3.5)$$

$$\mathbf{F}(t, \mathbf{x}, \mathbf{v}) = \frac{q}{m} \mathbf{E}(t, \mathbf{x}), \quad \mathbf{E}(t, \mathbf{x}) = -\nabla_{\mathbf{x}} \phi(t, \mathbf{x}), \quad -\Delta_{\mathbf{x}} \phi = q \frac{\rho}{\epsilon_0}. \quad (3.6)$$

Here we restrict our study in 1D spatial space. The numerical scheme adopted in the x -direction is the standard finite volume discretization. Suppose Γ_h to be a uniform mesh in \mathbb{R} , and each cell is identified by an index j . For a fixed $x_0 \in \mathbb{R}$ and $\Delta x > 0$,

$$\Gamma_h = \{T_j = x_0 + (j\Delta x, (j+1)\Delta x) : j \in \mathbb{Z}\}. \quad (3.7)$$

The numerical solution which is the approximation of the distribution function f at $t = t_n$ is denoted as

$$f_h^n(x, \mathbf{v}) = f_j^n(\mathbf{v}), \quad x \in T_j, \quad (3.8)$$

where $f_j^n(\mathbf{v})$ is the approximation over the cell T_j at the n -th time step and has the following Hermite expansion form as

$$f_j^n(\mathbf{v}) = \sum_{|\alpha| \leq M} f_{\alpha,j}^n \mathcal{H}_{u_{th,j}^n, \alpha} \left(\frac{\mathbf{v} - \mathbf{u}_j^n}{\sqrt{u_{th,j}^n}} \right).$$

3.1 The convection step

The equation (3.1) is discretized as

$$f_j^{n+1,*}(\mathbf{v}) = f_j^n(\mathbf{v}) + K_{1,j}^n(\mathbf{v}) + K_{2,j}^n(\mathbf{v}), \quad (3.9)$$

where $K_{1,j}^n$ is the contribution of the term \mathcal{A}_{α} in (2.39) without considering the acceleration, and $K_{2,j}^n$ is the contribution of the term $\hat{\mathcal{B}}_{\alpha}$ in (2.39). Noticing that the term \mathcal{A}_{α}

results in the conservative part in the Grad-type moment system, its contribution $K_{1,j}^n$ is discretized in the conservative formation as

$$K_{1,j}^n(\mathbf{v}) = -\frac{\Delta t^n}{\Delta x} \left[F_{j+\frac{1}{2}}^n(\mathbf{v}) - F_{j-\frac{1}{2}}^n(\mathbf{v}) \right], \quad (3.10)$$

where $F_{j+\frac{1}{2}}^n$ is the numerical flux between cell T_j and T_{j+1} at t^n . We use the HLL scheme in our numerical experiments following [8], which reads:

$$F_{j+\frac{1}{2}}^n(\mathbf{v}) = \begin{cases} v_1 f_j^n(\mathbf{v}), & 0 \leq \lambda_{j+\frac{1}{2}}^L, \\ \frac{\lambda_{j+\frac{1}{2}}^R v_1 f_j^n(\mathbf{v}) - \lambda_{j+\frac{1}{2}}^L v_1 f_{j+1}^n(\mathbf{v}) + \lambda_{j+\frac{1}{2}}^L \lambda_{j+\frac{1}{2}}^R [f_{j+1}^n(\mathbf{v}) - f_j^n(\mathbf{v})]}{\lambda_{j+\frac{1}{2}}^R - \lambda_{j+\frac{1}{2}}^L}, & \lambda_{j+\frac{1}{2}}^L < 0 < \lambda_{j+\frac{1}{2}}^R, \\ v_1 f_{j+1}^n(\mathbf{v}), & 0 \geq \lambda_{j+\frac{1}{2}}^R, \end{cases} \quad (3.11)$$

where $\lambda_{j+\frac{1}{2}}^L$ and $\lambda_{j+\frac{1}{2}}^R$ are the fastest signal speeds [5] as

$$\begin{aligned} \lambda_{j+\frac{1}{2}}^L &= \min\{u_{1,j}^n - C_{M+1}\sqrt{u_{th,j}^n}, u_{1,j+1}^n - C_{M+1}\sqrt{u_{th,j+1}^n}\}, \\ \lambda_{j+\frac{1}{2}}^R &= \max\{u_{1,j}^n + C_{M+1}\sqrt{u_{th,j}^n}, u_{1,j+1}^n + C_{M+1}\sqrt{u_{th,j+1}^n}\}, \end{aligned} \quad (3.12)$$

where C_{M+1} is the greatest zero of $He_{M+1}(x)$, u_1 is the first component of the macroscopic velocity \mathbf{u} , and u_{th} is the thermal velocity. The formula of the signal speed is also used to determine the time step Δt^n by the CFL condition. Two points remain unclear in the numerical flux. The first one is how to calculate $v_1 f_j^n(\mathbf{v})$. This is managed according to the recursion relation of Hermite polynomials:

$$\begin{aligned} v_1 f_j^n(\mathbf{v}) &= [(u_{th,j}^n)^{1/2}(\xi_{1,j}^n) + (u_{1,j}^n)] \sum_{|\alpha| \leq M} f_{j,\alpha}^n \mathcal{H}_{j,\alpha}^n(\xi_j^n) \\ &= \sum_{|\alpha| \leq M} f_{j,\alpha}^n [u_{th,j}^n \mathcal{H}_{j,\alpha+e_1}^n(\xi_j^n) + (u_{1,j}^n) \mathcal{H}_{j,\alpha}^n(\xi_j^n) + \alpha_1 \mathcal{H}_{j,\alpha-e_1}^n(\xi_j^n)], \end{aligned} \quad (3.13)$$

where $\xi_j^n = (\mathbf{v} - \mathbf{u}_j^n)/\sqrt{u_{th,j}^n}$, $\xi_{1,j}^n$ is the first entry of ξ_j^n , and $\mathbf{u}_j^n, u_{th,j}^n$ are the mean macroscopic velocity and thermal velocity in the j -th cell. Since $|\alpha + e_1| = M + 1$ when $|\alpha| = M$, $v_1 f_j^n(\mathbf{v})$ no longer exists in the space $F_M(\mathbf{u}_j^n, u_{th,j}^n)$. By simply dropping the terms with $|\alpha + e_1| = M + 1$, we project $v_1 f_j^n(\mathbf{v})$ back into $F_M(\mathbf{u}_j^n, u_{th,j}^n)$, since when $|\alpha| > M$, $H_\alpha(\xi)$ is orthogonal to $F_M(\mathbf{u}, u_{th})$ with respect to the inner product

$$(f, g) = \int_{\mathbb{R}^3} f(\xi) g(\xi) \exp\left(-\frac{|\xi|^2}{2}\right) d\xi. \quad (3.14)$$

The other point is how to add up two distribution functions lying in $F_M(\mathbf{u}_j^n, u_{th,j}^n)$ and $F_M(\mathbf{u}_{j+1}^n, u_{th,j+1}^n)$ respectively. The proposition in [6] is referred to solve it.

Proposition 1. *Suppose $f \in F_M(\mathbf{u}_1, u_{th,1})$ can be represented by*

$$f(\mathbf{v}) = \sum_{|\alpha| \leq M} f_{1,\alpha} \mathcal{H}_{u_{th,1},\alpha}(\xi_1), \quad \xi_1 = (\mathbf{v} - \mathbf{u}_1)/\sqrt{u_{th,1}}. \quad (3.15)$$

For some $\mathbf{u}_2 \in \mathbb{R}^3$ and $u_{th,2} > 0$, $\{F_\alpha(\tau)\}_{|\alpha| \leq M}$ satisfies

$$\begin{cases} \frac{dF_\alpha}{d\tau} = \sum_{d=1}^3 S^2 [u_{th,1} R F_{\alpha-2e_d} + w_d \sqrt{u_{th,1}} F_{\alpha-e_d}], & \forall \tau \in [0, 1], \\ F_\alpha(0) = f_{1,\alpha}, \end{cases} \quad (3.16)$$

where S and R are given below. And $\mathbf{w} = (\mathbf{u}_1 - \mathbf{u}_2)/\sqrt{u_{th,2}}$, $\hat{u}_{th} = \sqrt{u_{th,1}/u_{th,2}}$.

$$R(\tau) = \frac{\hat{u}_{th} - 1}{(\hat{u}_{th} - 1)\tau + 1}, \quad S(\tau) = 1 - \tau R(\tau) = \frac{1}{(\hat{u}_{th} - 1)\tau + 1}. \quad (3.17)$$

Let

$$g(\mathbf{v}) = \sum_{|\alpha| \leq M} F_\alpha(1) \mathcal{H}_{u_{th,2}, \alpha}(\boldsymbol{\xi}_2), \quad \boldsymbol{\xi}_2 = (\mathbf{v} - \mathbf{u}_2)/\sqrt{u_{th,2}}. \quad (3.18)$$

Then $g(\mathbf{v}) \in F_M(\mathbf{u}_2, u_{th,2})$ and $g(\mathbf{v})$ satisfies

$$\int_{\mathbb{R}^3} p(\mathbf{v}) f(\mathbf{v}) d\mathbf{v} = \int_{\mathbb{R}^3} p(\mathbf{v}) g(\mathbf{v}) d\mathbf{v}, \quad \forall p(\mathbf{v}) \in P_M(\mathbb{R}^3). \quad (3.19)$$

The proposition provides an algorithm to project a function in $F_M(\mathbf{u}_1, u_{th,1})$ to the space $F_M(\mathbf{u}_2, u_{th,2})$. Assuming $f_1 \in F_M(\mathbf{u}_1, u_{th,1})$ and $f_2 \in F_M(\mathbf{u}_2, u_{th,2})$, we can find an $\tilde{f}_1 \in F_M(\mathbf{u}_2, u_{th,2})$ as a representation of $f_1 \in F_M(\mathbf{u}_1, u_{th,1})$ in the sense of (3.19). Thus, to add up $f_j \in F_M(\mathbf{u}_j^n, u_{th,j}^n)$ and $f_{j+1} \in F_M(\mathbf{u}_{j+1}^n, u_{th,j+1}^n)$, we first find an $\hat{f}_{j+1} \in F_M(\mathbf{u}_j^n, u_{th,j}^n)$ as an approximation of f_{j+1} in the sense of (3.19), and then add up the coefficients of f_j and \hat{f}_{j+1} for the same basis function.

The regularization term appears only in the moment equations containing $\partial f_\alpha / \partial t$ with $|\alpha| = M$. Therefore, only when $|\alpha| = M$, we have to calculate $K_{2,j}^n$. We simply use the central difference scheme to approximate the spatial derivatives in (2.38):

$$\begin{aligned} \frac{\partial u_d}{\partial x} &\approx \nabla_x^h u_{d,j}^n \triangleq \frac{u_{d,j+1}^n - u_{d,j-1}^n}{2\Delta x}, \\ \frac{\partial u_{th}}{\partial x} &\approx \nabla_x^h u_{th,j}^n \triangleq \frac{u_{th,j+1}^n - u_{th,j-1}^n}{2\Delta x}. \end{aligned} \quad (3.20)$$

Then we get the numerical approximation for $K_{2,j}^n$ with $|\alpha| = M$, as

$$K_{2,j}^n = -\Delta t \sum_{|\alpha|=M} (\alpha_1 + 1) \sum_{d=1}^3 \left(f_{\alpha-e_d+e_1}^n \nabla_x^h u_{d,j}^n + \frac{f_{\alpha-2e_d+e_1}^n}{2} \nabla_x^h u_{th,j}^n \right) \mathcal{H}_{u_{th,j}, \alpha} \left(\frac{\mathbf{v} - \mathbf{u}_j^n}{\sqrt{u_{th,j}^n}} \right). \quad (3.21)$$

3.2 The acceleration and collision step

The acceleration step is performed by solving

$$\frac{\partial u_1}{\partial t} - F_1 = 0. \quad (3.22)$$

For the time step Δt , (3.22) is approximated as

$$u_{1,j}^{n+1} = u_{1,j}^{n+1,*} + \Delta t F_{1,j}^{n+1}, \quad (3.23)$$

where $u_{1,j}^{n+1,*}$ is the first entry of the macroscopic velocity \mathbf{u} in the j -th cell after the convection step at $t = t^n$. And $F_{1,j}^{n+1}$ is the first entry of the electric force \mathbf{F} in the j -th cell after the convection step at $t = t^n$. In the 1D spatial space, the Poisson equation (2.2) reduces into a second order ODE as

$$F_1(t, x, \mathbf{v}) = \frac{q}{m} E_1(t, x), \quad E_1(t, x) = -\frac{\partial \psi(t, x)}{\partial x}, \quad -\partial_{xx} \psi = \frac{q\rho}{\epsilon_0}. \quad (3.24)$$

The three-point central difference scheme is used to discretize the potential equation

$$-\frac{\psi_{j+1}^{n+1} - 2\psi_j^{n+1} + \psi_{j-1}^{n+1}}{\Delta x^2} = \frac{q\rho_j^{n+1}}{\epsilon_0}, \quad (3.25)$$

where ρ_j^{n+1} is the density in the j -th cell after the convection step, noticing that the density is not updated in the acceleration step and the collision step. The central difference is used to approximate $E_{1,j}^{n+1}$ and $F_{1,j}^{n+1}$

$$E_{1,j}^{n+1} = -\frac{\psi_{j+1}^{n+1} - \psi_{j-1}^{n+1}}{2\Delta x}, \quad F_{1,j}^{n+1} = \frac{q}{m} E_{1,j}^{n+1}. \quad (3.26)$$

For the BGK collision model, the moment expansion results in a simple form (2.16), and (3.4) changes into

$$\frac{\partial f_\alpha}{\partial t} = -\nu f_\alpha, \quad |\alpha| \geq 2. \quad (3.27)$$

It is directly integrated as

$$f_{j,\alpha}^{n+1} = f_{j,\alpha}^{n+1,*} \exp(-\nu \Delta t^n), \quad \forall \alpha \in \mathbb{N}^3, \quad 1 < |\alpha| \leq M. \quad (3.28)$$

Remark 3. The collision step only revises the coefficients with $2 \leq |\alpha| \leq M$, and does not change the macroscopic velocity \mathbf{u} and the density ρ , which are decided by the coefficients with $|\alpha| < 2$.

3.3 Outline of the algorithm

The overall numerical scheme is summarized as below:

1. Let $n = 0$ and set the initial value of $f_{j,\alpha}^n$;
2. Calculate Δt^n according to the CFL condition;
3. Integrate the convection term using (3.9);
4. Update the macroscopic velocity using (3.26) and (3.23);
5. Apply the collision step (3.28);
6. Let $n \leftarrow n + 1$, and return to step 2.

Remark 4. For the V-P equation, $\nu = 0$, and the collision step is simply skipped over.

The scheme keeps both the discretized mass and momentum conserved. Precisely, in the case of the periodic boundary condition, let us denote the discretized mass as

$$\mathcal{D}_h(t_n) = \sum_{j=1}^N \Delta x \int_{\mathbf{v} \in \mathbb{R}^3} f_j^n(\mathbf{v}) d\mathbf{v} \quad (3.29)$$

and discretized momentum as

$$\mathcal{M}_h(t_n) = \sum_{j=1}^N \Delta x \int_{\mathbf{v} \in \mathbb{R}^3} \mathbf{v} f_j^n d\mathbf{v}, \quad (3.30)$$

we have the following conclusion.

Theorem 1. *The numerical solution $f_h^n(x, \mathbf{v})$ given by the algorithm above in the case of the periodic boundary condition satisfies that*

$$\mathcal{D}_h(t_n) = \mathcal{D}_h(t_0), \quad \mathcal{M}_h(t_n) = \mathcal{M}_h(t_0) \quad (3.31)$$

for all $n > 0$.

Proof. Noticing that the mass on each cell is not modified when we apply the regularization term and in the acceleration step, the conservation of the mass is straight forward based on results in [8].

The momentum conservation is equivalent to verify

$$\mathcal{M}_h(t_{n+1}) = \mathcal{M}_h(t_n). \quad (3.32)$$

It is clear that the collision step does not change the macroscopic velocity and the density. Therefore we verify below that the momentum is conserved in the acceleration step and the convection step, respectively.

1. We first verify that the acceleration step keeps momentum conservation. From (2.6) and (3.23), we have

$$\begin{aligned} \mathcal{M}_h(t_{n+1}) &= \sum_{j=1}^N \Delta x \int_{\mathbf{v} \in \mathbb{R}^3} \mathbf{v} f_j^{n+1} d\mathbf{v} \\ &= \Delta x \sum_{j=1}^N \rho_j^{n+1} \mathbf{u}_j^{n+1} \\ &= \Delta x \sum_{j=1}^N \rho_j^{n+1} (\mathbf{u}_j^{n+1,*} + \mathbf{F}_j^{n+1} \Delta t^n) \\ &= \Delta x \sum_{j=1}^N \rho_j^{n+1} \mathbf{u}_j^{n+1,*} + \Delta x \Delta t^n \sum_{j=1}^N \mathbf{F}_j^{n+1} \rho_j^{n+1}. \end{aligned} \quad (3.33)$$

According to (3.25) and (3.26), we have

$$\begin{aligned} \sum_{j=1}^N F_{1,j}^{n+1} \rho_j^{n+1} &= \sum_{j=1}^N \left(-\frac{\epsilon_0}{q} \right) \frac{\psi_{j+1} - 2\psi_j + \psi_{j-1}}{\Delta x^2} \left(-\frac{q}{m} \right) \frac{\psi_{j+1} - \psi_{j-1}}{2\Delta x} \\ &= \frac{\epsilon_0}{2m\Delta x^3} \sum_{j=1}^N (\psi_{j+1}\psi_{j+1} - \psi_{j-1}\psi_{j-1} - 2\psi_j\psi_{j+1} \\ &\quad + 2\psi_j\psi_{j-1} + \psi_{j-1}\psi_{j+1} - \psi_{j+1}\psi_{j-1}) \\ &= \psi_N^2 + \psi_{N+1}^2 - \psi_0^2 - \psi_1^2 + \psi_0\psi_1 - \psi_N\psi_{N+1}. \end{aligned} \quad (3.34)$$

Since we restrict the problem to the 1D spatial space with the periodic boundary condition, we deduce by $\psi_{N+1} = \psi_1$, $\psi_0 = \psi_N$, $F_2 \equiv 0$ and $F_3 \equiv 0$ that

$$\sum_{j=1}^N \mathbf{F}_j^{n+1} \rho_j^{n+1} = 0,$$

and we obtain

$$\mathcal{M}_h(t_{n+1}) = \Delta x \sum_{j=1}^N \rho_j^{n+1} \mathbf{u}_j^{n+1,*}. \quad (3.35)$$

Since ρ_j^{n+1} is the density after the n -th convection step, $\Delta x \sum_{j=1}^N \rho_j^{n+1} \mathbf{u}_j^{n+1,*}$ is the total momentum after the n -th convection step.

2. Here we verify that the convection step does not change the total momentum. Thanks to (2.6) and (3.9), we have

$$\begin{aligned} \Delta x \sum_{j=1}^N \rho_j^{n+1} \mathbf{u}_j^{n+1,*} &= \sum_{j=1}^N \Delta x \int_{\mathbf{v} \in \mathbb{R}^3} \mathbf{v} f_j^{n+1,*} d\mathbf{v} \\ &= \sum_{j=1}^N \Delta x \int_{\mathbf{v} \in \mathbb{R}^3} \mathbf{v} [f_j^n + K_{1,j}^n + K_{2,j}^n] d\mathbf{v} \\ &= \sum_{j=1}^N \Delta x \int_{\mathbf{v} \in \mathbb{R}^3} \mathbf{v} f_j^n d\mathbf{v} + \sum_{j=1}^N \Delta x \int_{\mathbf{v} \in \mathbb{R}^3} \mathbf{v} K_{1,j}^n d\mathbf{v} + \sum_{j=1}^N \Delta x \int_{\mathbf{v} \in \mathbb{R}^3} \mathbf{v} K_{2,j}^n d\mathbf{v} \\ &= \sum_{j=1}^N \Delta x \int_{\mathbf{v} \in \mathbb{R}^3} \mathbf{v} f_j^n d\mathbf{v} - \Delta t^n \sum_{j=1}^N \int_{\mathbf{v} \in \mathbb{R}^3} \mathbf{v} (F_{j+1/2}^n - F_{j-1/2}^n) d\mathbf{v} + \sum_{j=1}^N \Delta x \int_{\mathbf{v} \in \mathbb{R}^3} \mathbf{v} K_{2,j}^n d\mathbf{v} \\ &= \mathcal{M}_h(t_n) - \Delta t^n \int_{\mathbf{v} \in \mathbb{R}^3} \mathbf{v} (F_{N+1/2}^n - F_{1/2}^n) d\mathbf{v} + \sum_{j=1}^N \Delta x \int_{\mathbf{v} \in \mathbb{R}^3} \mathbf{v} K_{2,j}^n d\mathbf{v}. \end{aligned} \quad (3.36)$$

Due to the periodic boundary condition, we have that $F_{N+1/2}^n = F_{1/2}^n$. Meanwhile, the regularization part only updates the M -th order terms which have no effect on the macroscopic velocity \mathbf{u} and the density ρ , thus the regularization term will not break the momentum conservation. Precisely speaking, the basis functions of $K_{2,j}$ are $\mathcal{H}_{u_{th,j}^n, \alpha} \left((\mathbf{v} - \mathbf{u}_j^n) / \sqrt{u_{th,j}^n} \right)$, with $|\alpha| = M$, $M \geq 3$, which are orthogonal to \mathbf{v} , then

$$\int_{\mathbf{v} \in \mathbb{R}^3} \mathbf{v} K_{2,j}^n d\mathbf{v} = 0, \quad (3.37)$$

and we obtain

$$\Delta x \sum_{j=1}^N \rho_j^{n+1} \mathbf{u}_j^{n+1,*} = \mathcal{M}_h(t_n). \quad (3.38)$$

With (3.35) and (3.38), we conclude the total momentum conservation consequently

$$\mathcal{M}_h(t_{n+1}) = \mathcal{M}_h(t_n). \quad (3.39)$$

This ends the proof. \square

4 Numerical Examples

We study the linear Landau damping modelled by the V-P and V-B equations with the periodic boundary conditions. The CFL number is always set as 0.45. The specific examples are from [10]. The form of the V-B equations with the periodic boundary conditions coupled with the normalized Poisson equation is

$$\frac{\partial f}{\partial t} + \mathbf{v} \cdot \nabla_x f + E \cdot \nabla_{\mathbf{v}} f = \nu(f_M - f), \quad (4.1)$$

$$E(t, x) = -\nabla_x \psi(t, x), \quad (4.2)$$

$$-\Delta \psi(t, x) = \int_{\mathbb{R}^3} f(t, x, \mathbf{v}) d\mathbf{v} - 1. \quad (4.3)$$

Here we adopt the same initial data as in [10]

$$f(0, x, \mathbf{v}) = f_M = \frac{1}{\sqrt{2\pi}} e^{-|\mathbf{v}|^2/2} (1 + A \cos(kx)), \quad (x, \mathbf{v}) \in (0, L) \times \mathbb{R}^3, \quad (4.4)$$

where A is the amplitude of the perturbation, k denotes the wave number, and the periodic length is taken as $L = 2\pi/k$. The initial data and (2.35) give us

$$\rho(0, x) = f_0(0, x) = (1 + A \cos(kx)), \quad f_\alpha|_{t=0} = 0, \quad |\alpha| > 0. \quad (4.5)$$

What of one's interests is the evolution of the square root of the electric energy, which is defined as

$$\mathcal{E}_h(t) = \sum_{j=1}^N \Delta x E_j^2(t). \quad (4.6)$$

According to Landau's theory, the time evolution of the square root of $\mathcal{E}_h(t)$ is expected to be exponentially decaying almost with a fixed rate γ_L , which is affected by the wave number k and the collision frequency ν . For this purpose, we always plot the square root of $\mathcal{E}_h(t)$ in logarithm scale in the figures in this section. The total energy is the sum of the electric energy and the kinetic and internal energy of the particles as

$$\mathcal{E}_{total}(t) = \mathcal{E}_h(t) + \mathcal{E}_p(t), \quad (4.7)$$

where the kinetic and internal energy of the particles

$$\mathcal{E}_p(t) = \Delta x \sum_{i=1}^N (\rho_i(t) u_i^2(t) + \rho_i(t) u_{th,i}(t)). \quad (4.8)$$

4.1 Numerical resolution study

We first examine the numerical convergence on different spatial grid size. The V-P equations in 1D spatial space and 1D velocity space are numerically solved. The number of moments is set as 80. In Figure 1, the evolution of the square root of $\mathcal{E}_h(t)$ with the wave numbers $k = 0.3, 0.5$ on different grid size is presented. The number of spatial grids we used are 500, 1000, 2000, 4000 and 8000. It is clear that the square root of $\mathcal{E}_h(t)$ is damping exponentially on all different grid size. With the increasing of the grid number, the damping rate is decreasing monotonically. For the spatial grid size Δx , we adopt the least square fitting, which uses the peak value points of $\mathcal{E}_h(t)$, to obtain the numerical

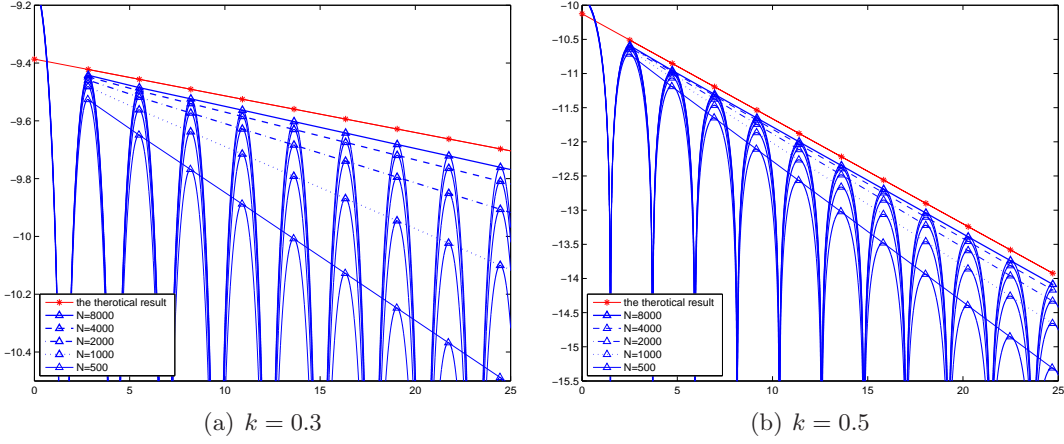


Figure 1: Exponentially damping in time of the square root of \mathcal{E}_h on different spatial grids with the wave number $k = 0.3$ and 0.5 . The curves in blue are the square root of \mathcal{E}_h in time using logarithm scale on different spatial grid size. The slopes of the blue lines are the numerical damping rate γ_L^h by the least square fitting of the peak value points of \mathcal{E}_h . The slope of the red line is the damping rate given by the theoretic data in Table 1.

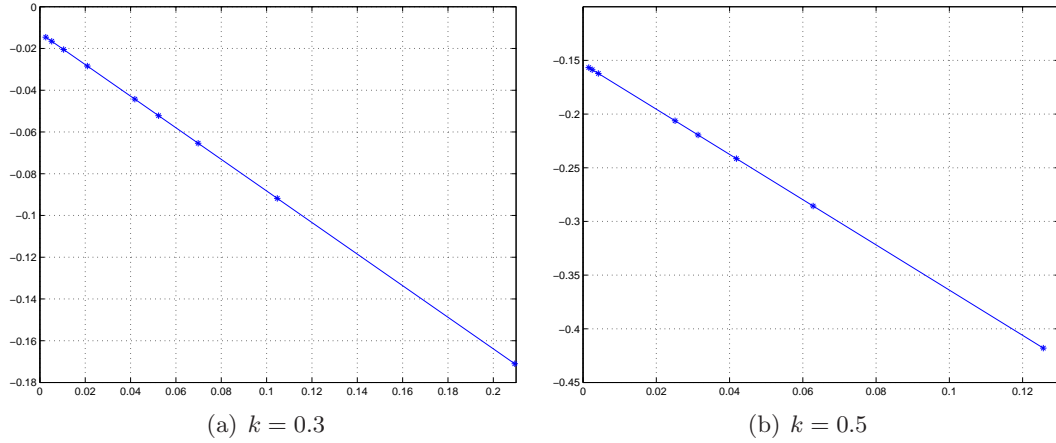


Figure 2: The linear dependence of the numerical damping rates in spatial grid size with the wave number $k = 0.3$ and 0.5 . The x -axis is the spatial grid size Δx and the y -axis is numerical damping rate $\gamma_L^h(\Delta x)$. The line is obtained by the least square fitting of $\gamma_L^h(\Delta x)$ with Δx ranging from $L/100$ to $L/8000$. The intercept of the line on y -axis is the parameter $\gamma_L^{h,0}$ and the slope of the line is the parameter $\gamma_L^{h,1}$.

damping rate γ_L^h . One finds obviously in Figure 1 that both $\mathcal{E}_h(t)$ and the damping rate γ_L^h are converging while the spatial grid size Δx is going to zero. Furthermore, if we take the numerical damping rate γ_L^h as a function of the spatial grid size Δx and apply a least square fitting to retrieve the parameters $\gamma_L^{h,0}$ and $\gamma_L^{h,1}$ (see Figure 2) in the ansatz as

$$\gamma_L^h(\Delta x) = \gamma_L^{h,0} + \gamma_L^{h,1} \Delta x,$$

it is found that the fitting provides us both parameters extremely close to constants for all the values of k we tested ranging from 0.2 to 0.5 . This indicates us that the following

relation

$$\gamma_L^h(\Delta x) - \gamma_L^{h,0} \propto \Delta x \quad (4.9)$$

is approximately valid. The obtained parameter $\gamma_L^{h,0}$ is regarded as the limit of the numerical damping rate when Δx is going to zero. To our surprise, the limit $\gamma_L^{h,0}$ we obtained is in perfect agreement with the theoretic data in Table 1.

Wave number k	Theoretic data [14]	$\gamma_L^{h,0}$
0.2	-5.5×10^{-5}	-9.28×10^{-5}
0.3	-0.0126	-0.01260
0.4	-0.0661	-0.06614
0.5	-0.1533	-0.15334

Table 1: The comparison of the limit numerical damping rates and the theoretic data.

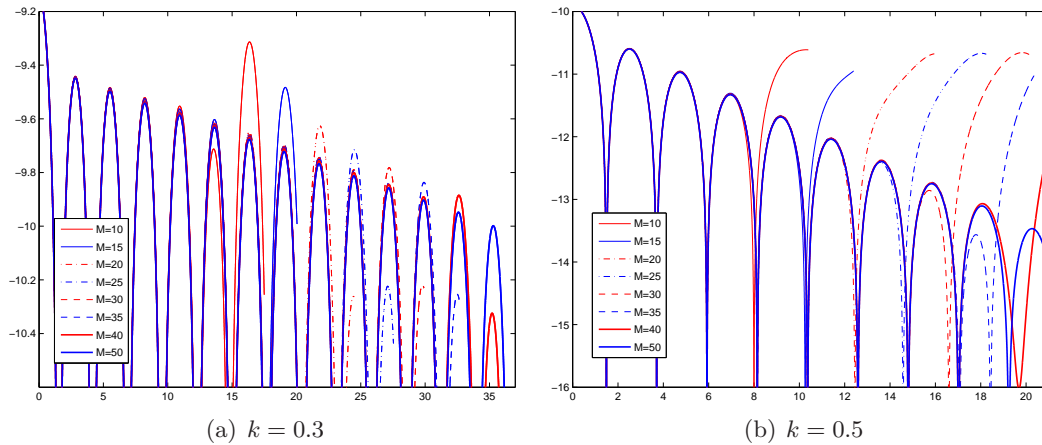


Figure 3: Exponentially damping in time of the square root of \mathcal{E}_h on different number of moments M with the wave number $k = 0.3$ and 0.5 . The curves are the square root of \mathcal{E}_h in time using logarithm scale using different number of moments.

Let us turn to the study of the numerical convergence in term of the number of moments. Again the V-P equations in 1D spatial space and 1D velocity space are numerically solved. The results using different number of moments ranging from 10 to 50 are collected in Figure 3 with fixed number of spatial grids. In this figure, we observe that the behavior of the time evolution of $\mathcal{E}_h(t)$ for different number of moments are almost the same at the beginning, indicating that the numerical damping rates are very close to each other. The damping of the square root of $\mathcal{E}_h(t)$ is persisting until the recurrence appears. After the appearance of the recurrence, the evolving of $\mathcal{E}_h(t)$ deviates evidently from exponentially decaying.

The exponential convergence rate in the number of moments is expected since the Hermite spectral expansion is used in the velocity space. We notice that the exponential convergence in term of number of moments is quite different to be observed, since the numerical error is in linear convergence due to the dominance of the spatial discretization. As the best try, a very fine spatial grid with 8000 points, which is about the maximal capacity of our current hardware, is used in the computation to suppress the spatial discretization error. With the fixed spatial grid size, we then take the numerical damping rate γ_L^h as a

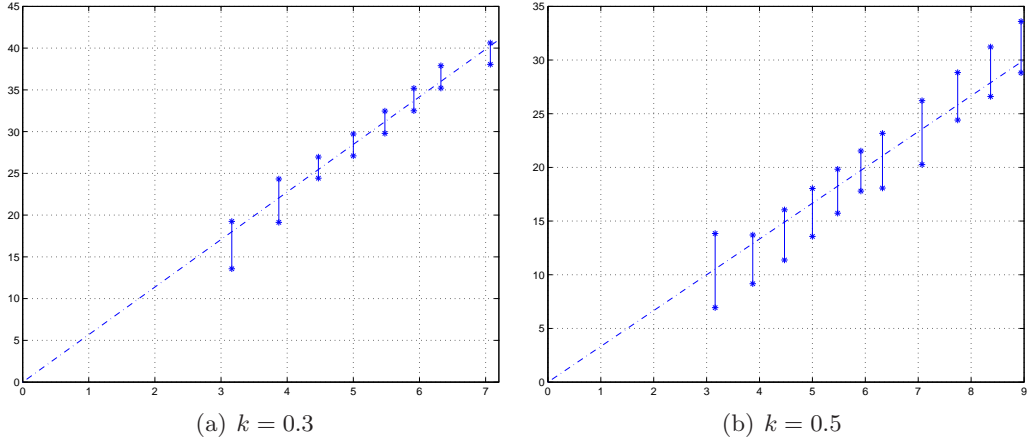


Figure 4: The dependence of the recurrence time on the number of moments used. The x -axis is the square root of the number of moments M , and the y -axis is time. The recurrence time for a given M is between the time of the sequential peak values of \mathcal{E}_h before and after it deviates from the exponentially decay (see Figure 3). In the figures, the vertical line segments are given by two time of the sequential peak values.

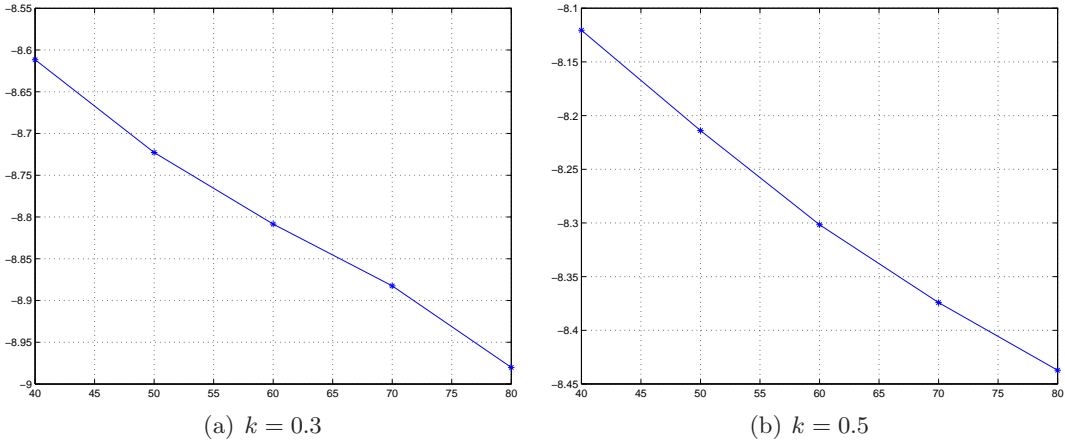


Figure 5: The approximately exponential convergence of the numerical damping rates in the number of moments with the wave number $k = 0.3$ and 0.5 . The x -axis is the number of moments M , with $M_i = 40, 50, 60, 70, 80, 90$ and $\Delta M = 10$. The y -axis is $\log(\gamma_L^h(M_i) - \gamma_L^h(M_{i-1}))$, where $\gamma_L^h(M_i)$ is obtained by the least square fitting of the peak values of \mathcal{E}_h . The spatial grid size is fixed as $\Delta x = L/8000$.

function of the number of moments M . In the case of an exponential convergence, the dependence of $\gamma_L^h(M)$ on M is as

$$\gamma_L^h(M) = \gamma_L^{m,0} + \gamma_L^{m,1} \lambda^{-M}, \quad (4.10)$$

where $\gamma_L^{m,0}$, $\gamma_L^{m,1}$ and λ are parameters independent of M . Let M_i be a given arithmetic sequence with a const $\Delta M = M_i - M_{i-1}$. Based on the ansatz (4.10), we have that

$$\begin{aligned} \gamma_L^h(M_i) &= \gamma_L^{m,0} + \gamma_L^{m,1} \lambda^{-M_i}, \\ \gamma_L^h(M_{i-1}) &= \gamma_L^{m,0} + \gamma_L^{m,1} \lambda^{-M_{i-1}}. \end{aligned}$$

By subtracting the two equations and then taking a logarithm on both sides, we have

$$\log\left(\gamma_L^h(M_i) - \gamma_L^h(M_{i-1})\right) = -M_i \log(\lambda) + \log \gamma_L^{m,1}(1 - \lambda^{\Delta M}).$$

It is to find that $\log(\gamma_L^h(M_i) - \gamma_L^h(M_{i-1}))$ is approximately linear in M_i if (4.10) is valid. We give the plot of $\log(\gamma_L^h(M_i) - \gamma_L^h(M_{i-1}))$ in M_i for $M_i = 40, 50, 60, 70, 80,$ and 90 in Figure 5. It is clear in this figure that $\log(\gamma_L^h(M_i) - \gamma_L^h(M_{i-1}))$ is almost linearly related with M_i , indicating that (4.10) is valid and the numerical convergence rate in term of the number of moments is approximately exponential.

It has been pointed out in [14] that the recurrence is an essential phenomenon of a class of numerical methods for the Vlasov equations. Such a phenomenon is mainly the effect of the free streaming part of the Vlasov equation. In the 1D case, it is

$$\frac{\partial f}{\partial t} + v \frac{\partial f}{\partial x} = 0. \quad (4.11)$$

It is not difficult to find that for any velocity v_i , we have $f(jL/v_i, x, v_i) = f(0, x, v_i)$ for an arbitrary integer j when the periodic boundary condition is imposed. Therefore, if a numerical scheme approximates the distribution function by taking its values on v_0, \dots, v_M in the velocity space, then, for a time T such that most of $T/(L/v_i)$, $i = 0, \dots, M$ are close to some positive integers, the discrete distribution function $f(T, x, v)$ will be close to the initial setting $f(0, x, v)$. Thus the recurrence occurs.

Our method is not able to escape away from this trap, either, since as pointed out in [5], the hyperbolic moment equation is similar as a discrete velocity model with a shifted and scaled stencil. Based on our observation in Figure 4, it is conjectured that the recurrence time is proportional to the square root of the moment expansion order M . For a finite difference discretisation in the velocity space, the recurrence time is proportional to the grid size in \mathbf{v} [14]. Noticing that the minimal distance between the zeros of M -th degree Hermite polynomial is around \sqrt{M} , the linear dependence of the recurrence time on \sqrt{M} consists with the analysis in [14] if we regard the moment method as a collocation spectral method in the velocity space with the collocation points being the zeros of Hermite polynomial.

It has been proved in Theorem 1 that the mass and the momentum are conserved by our scheme, while the total energy is not conserved. To examine the behavior of the total energy of our method, we present in Figure 6 the variation of the total energy in time in several different setups. It is clear that the total energy of the numerical solution produced by our method is changed very slightly in the whole computation.

4.2 Parameter study of linear Landau damping

The Landau damping with different wave numbers and collision frequencies are studied in this section. It is found that the numerical phenomena here are exactly the same as the collisionless case presented in Section 4.1, for the wave numbers ranging from 0.2 to 0.5 and the collision frequencies ranging from 0.01 to 0.05. We have checked the numerical convergence both in spatial grid size and order of moment expansion, and satisfied results are obtained. In all cases, the exponential damping of the square root of $\mathcal{E}_h(t)$ is observed.

Let us study the behavior of the solution with different wave numbers firstly. We use 3000 spatial grids and 80 moments to compute the evolution of $\mathcal{E}_h(t)$ for the wave numbers $k = 0.2, 0.3, 0.4,$ and 0.5 with the collision frequency $\nu = 0$, and the results are in Figure

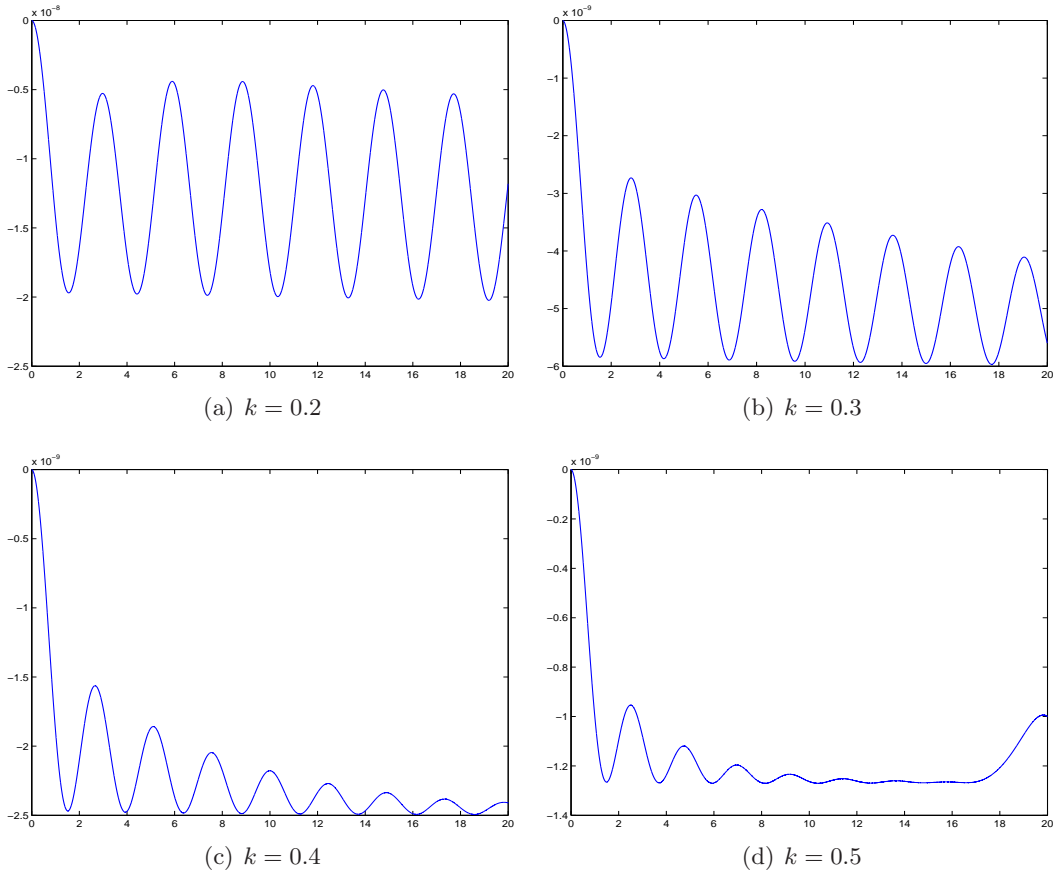


Figure 6: The variation of the total energy \mathcal{E}_{total} in time in the collisionless case with the wave number $k = 0.2, 0.3, 0.4$ and 0.5 . The x -axis is time and the y -axis is $\mathcal{E}_{total}(t) - \mathcal{E}_{total}(0)$. Noticing that $\mathcal{E}_{total}(0)$ is of $O(1)$, it is clear that the variation is very small, though the total energy is not conserved.

7. It is clear the $\mathcal{E}_h(t)$ is damping exponentially in time and the damping rate is increasing with greater wave number. This consists with the empirical formula given in [10].

In Figure 8, the evolution of the square root of \mathcal{E}_h with the wave number $k = 0.2, 0.3, 0.4$ and 0.5 with the collision frequency $\nu = 0.01$ is presented. We find that $\mathcal{E}_h(t)$ is also damping exponentially but with greater rates than that in the collisionless case. In Figure 9, the numerical results for the wave number $k = 0.2, 0.3, 0.4$ and 0.5 with a greater collision frequency $\nu = 0.05$ are plot. We find that $\mathcal{E}_h(t)$ is damping exponentially with an even greater rate than that in the case of $\nu = 0.01$. This consists again with the empirical formula given in [10], though a different collision term was used therein.

We numerically solve the V-B equations in 1D spatial space and 1D velocity space with the number of moments fixed as 80. The number of the spatial grids is ranging form 100 to 8000. The least square fitting of the peak value points is again adopted to get the numerical damping rate of the square root of \mathcal{E}_h for different Δx . In Figure 10, the damping rates for the wave numbers $k = 0.3, 0.5$, and the collision frequencies $\nu = 0.01, 0.05$ are plotted. It is clear that the numerical damping rates are all in a linearly and monotonically converging pattern with the spatial grid size Δx going to zero. Remember that in the collisionless case, the numerical damping rate is monotonically linearly converging to the theoretic

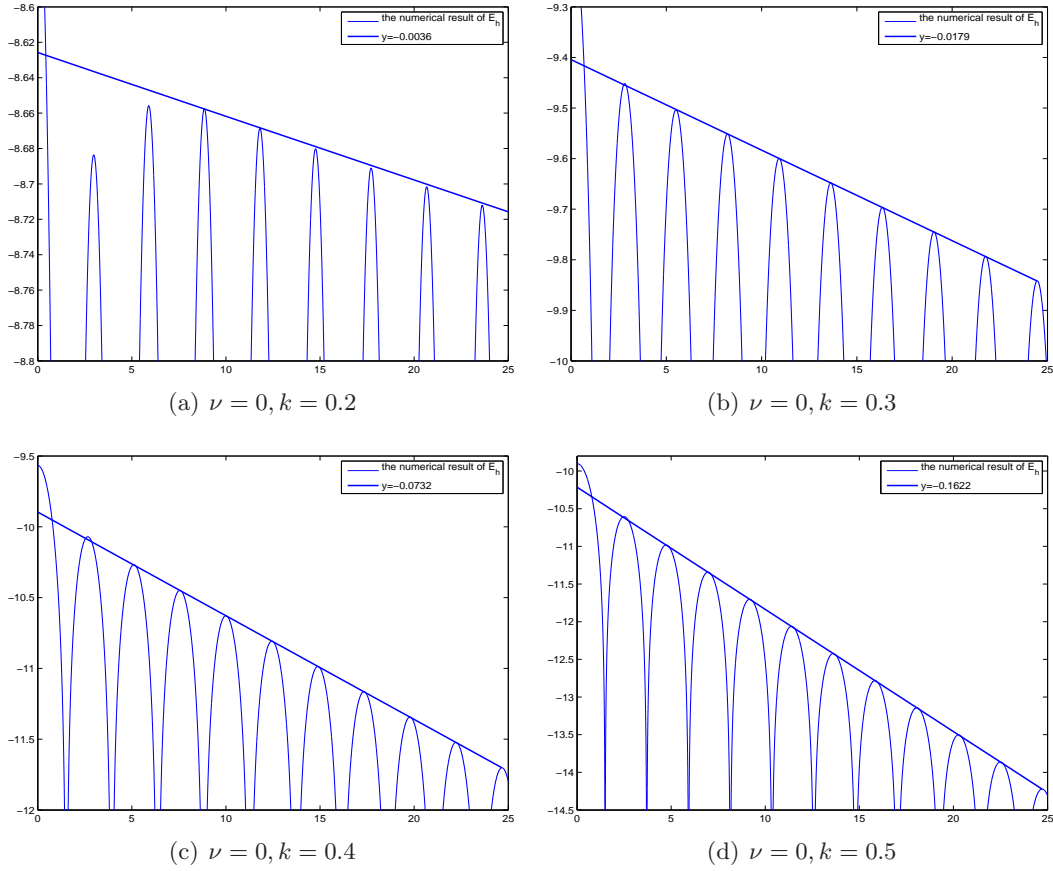


Figure 7: The dependence of the damping rate on the wave number k in the collisionless case. The curves are the evolving of the square root of \mathcal{E}_h in time using logarithm scale. The slope of the line is obtained by the least square fitting.

data with the spatial grid size going to zero. Based on such similarity, it is reasonable to conjecture that the damping rate with the collision term as the function of the spatial grid size is monotonically linearly converging to the exact damping rate while the spatial grid size is going to zero, too. This inspires us to predict the exact damping rate for different collision frequencies by the extrapolation of the numerical damping rates, which is the same as the approach in the collisionless case. We adopt the formula (4.9) again to retrieve the parameters by least square fitting. The obtained parameter $\gamma_L^{h,0}$ is regarded as the prediction of the exact damping rate. In Table 2, we present $\gamma_L^{h,0}$ for the wave numbers $k = 0.2, 0.3, 0.4,$ and 0.5 with $\nu = 0.01$ and 0.05 .

5 Concluding remarks

The NRxx method has been extended to solve the V-P and V-B equations. The method is able to capture the linear Landau damping effectively. We attempt to predict the exact Landau damping rates with the collision term based on our observation in the collisionless case.

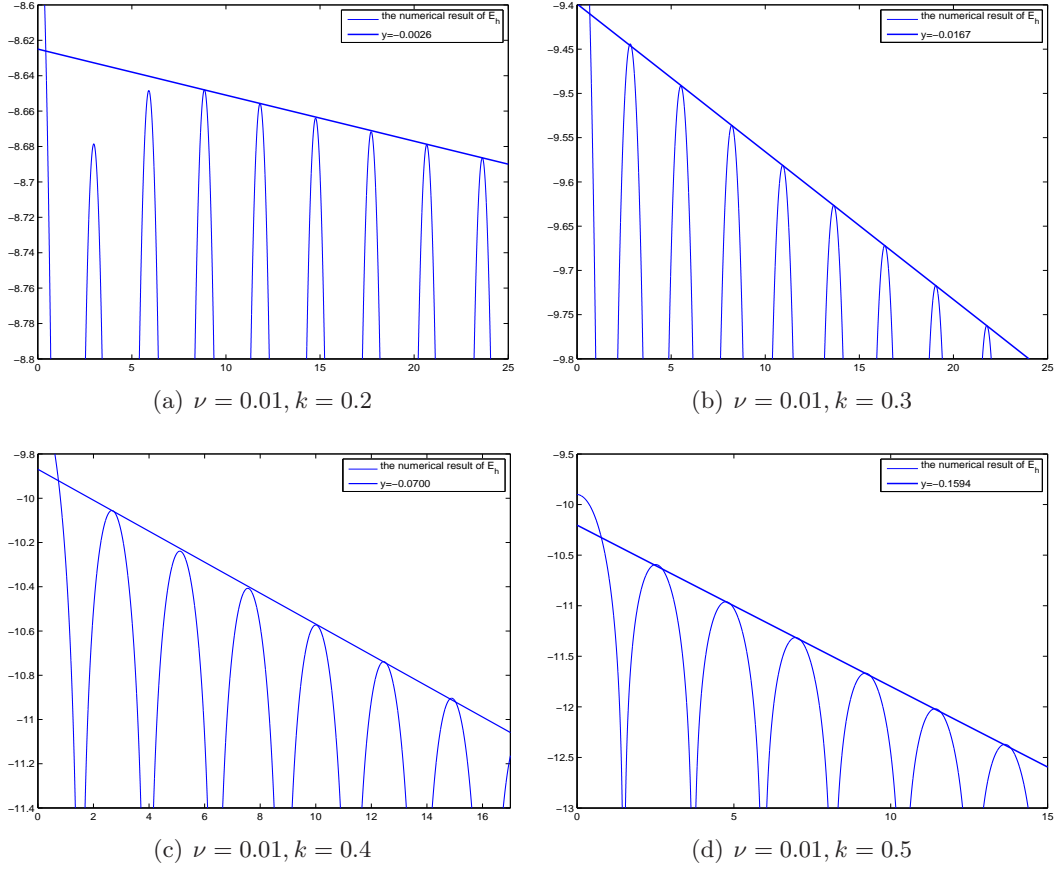


Figure 8: The dependence of the damping rate on the wave number k with collision frequency $\nu = 0.01$. The curves are the evolving of the square root of \mathcal{E}_h in time using logarithm scale. The slope of the line is obtained by the least square fitting.

Collision frequency ν	Wave number k	$\gamma_L^{h,0}$
0.01	0.2	-8.3796×10^{-5}
	0.3	-0.01361
	0.4	-0.06701
	0.5	-0.15331
0.05	0.2	-0.002094
	0.3	-0.01755
	0.4	-0.06966
	0.5	-0.15230

Table 2: The prediction of the linear Landau damping rates.

Acknowledgements

This research was supported in part by the National Basic Research Program of China (2011CB309704) and the Fok Ying Tong Education and NCET in China.

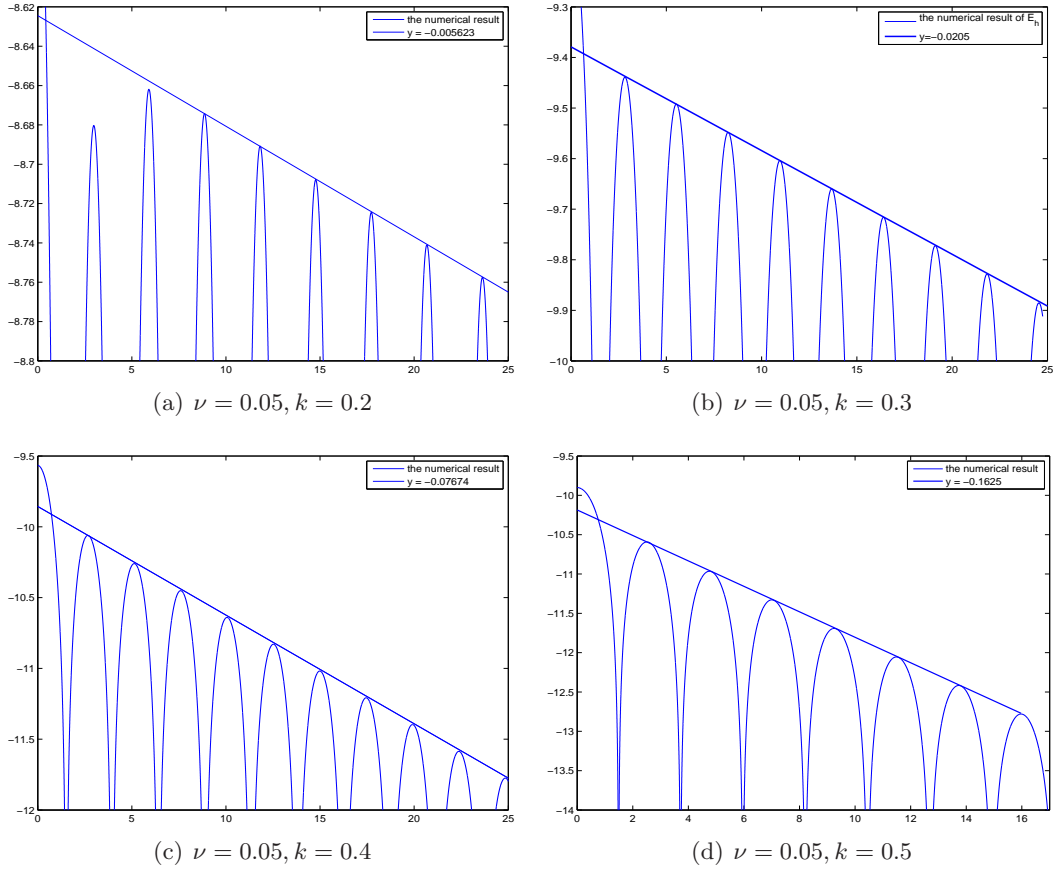


Figure 9: The dependence of the damping rate on the wave number k with collision frequency $\nu = 0.05$. The curves are the evolving of the square root of \mathcal{E}_h in time using logarithm scale. The slope of the line is obtained by the least square fitting.

References

- [1] P. L. Bhatnagar, E. P. Gross, and M. Krook. A model for collision processes in gases. I. small amplitude processes in charged and neutral one-component systems. *Phys. Rev.*, 94(3):511–525, 1954.
- [2] P. L. Bhatnagar, E. P. Gross, and M. Krook. Model for collision processes in gases: Small-amplitude oscillations of charged two-component systems. *Phys. Rev.*, 102(3):593–604, 1956.
- [3] C. K. Birdsall and A. B. Langdon, editors. *Plasma Physics via Computer Simulation*. Inst. of Phys. Publishing, Bristol/Philadelphia, 1991.
- [4] Z. Cai, Y. Fan, and R. Li. Globally hyperbolic regularization of Grad’s moment system. *To appear in Comm. Pure Appl. Math.*, 2012.
- [5] Z. Cai, Y. Fan, and R. Li. Globally hyperbolic regularization of Grad’s moment system in one dimensional space. *To appear in J. Math. Sci.*, 2012.
- [6] Z. Cai and R. Li. Numerical regularized moment method of arbitrary order for Boltzmann-BGK equation. *SIAM J. Sci. Comput.*, 32(5):2875–2907, 2010.

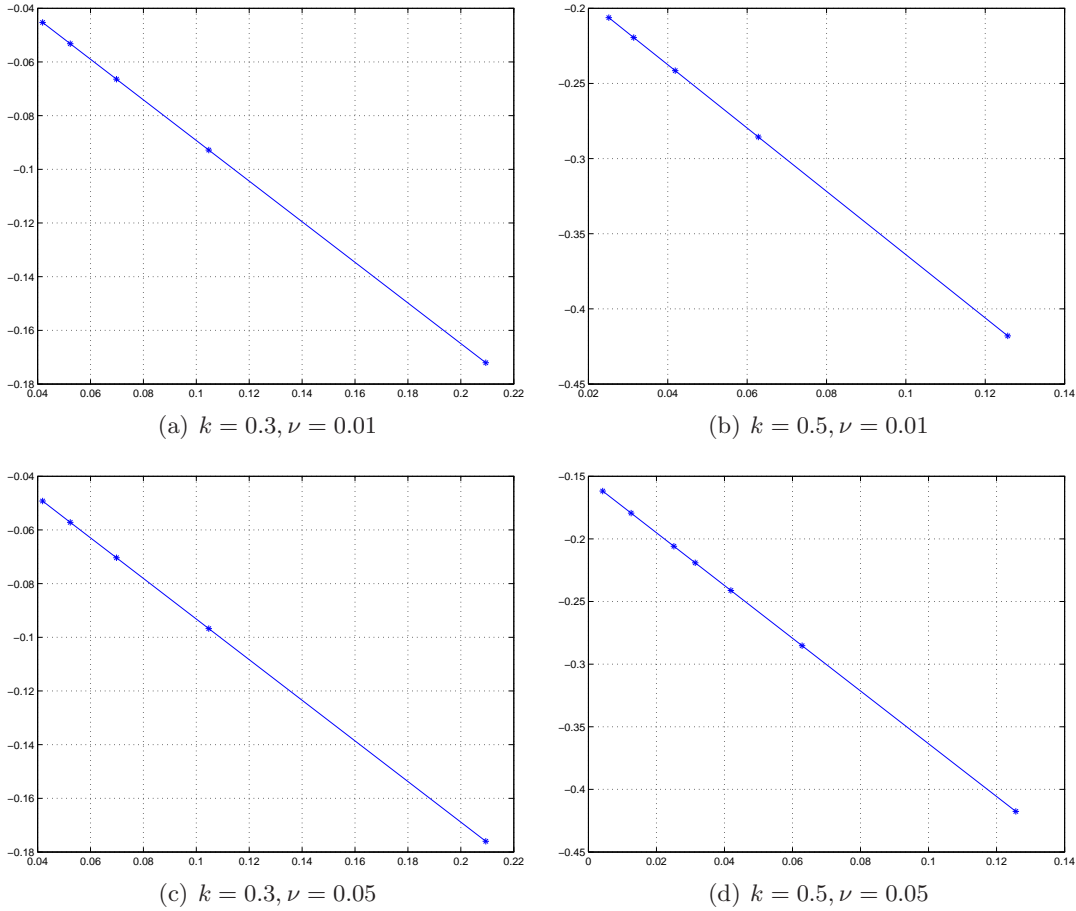


Figure 10: The prediction of the exact damping rate using extrapolation (4.9). The x -axis is the spatial grid size Δx and the y -axis is numerical damping rates $\gamma_L^h(\Delta x)$.

- [7] Z. Cai, R. Li, and Z. Qiao. NRxx simulation of microflows with Shakhov model. *SIAM J. Sci. Comput.*, 34(1):A339–A369, 2012.
- [8] Z. Cai, R. Li, and Y. Wang. An efficient NRxx method for Boltzmann-BGK equation. *J. Sci. Comput.*, 50(1):103–119, 2012.
- [9] Z. Cai, R. Li, and Y. Wang. Numerical regularized moment method for high Mach number flow. *Commun. Comput. Phys.*, 11(5):1415–1438, 2012.
- [10] N. Crouseilles and F. Filbet. Numerical approximation of collisional plasmas by high order methods. *J. Comput. Phys.*, 201(2):546–572, 2004.
- [11] M. Hénon. Vlasov equation? *Astronomy and Astrophysics*, 114(1):211–212, 1984.
- [12] T. Nakamura and T. Yabe. Cubic interpolated propagation scheme for solving the hyper-dimensional Vlasov-Poisson equation in phase space. *Comput. Phys. Commun.*, 120:122–154, 1999.
- [13] J. W. Schumer and J. P. Holloway. Vlasov simulation using velocity-scaled Hermite representations. *J. Comput. Phys.*, 144(2):626–661, 1998.

- [14] E. Sonnendrücker. Approximation numérique des équations de Vlasov-Maxwell. *Notes du cours de M2*, 2010.
- [15] E. Sonnendrücker, J. Roche, P. Bertrand, and A. Ghizzo. The semi-Lagrangian method for the numerical resolution of Vlasov equations. *J. Comput. Phys.*, 149(2):201–220, 1998.
- [16] A. A. Vlasov. On vibration properties of electron gas. *J. Exp. Theor. Phys.*, 8(3):291, 1938.
- [17] G. Vojta and M. Mocker. Eigenfunctions of the linearized Vlasov-BGK operator. *Phys. Letters A*, 30(5):303–304, 1969.
- [18] G. Vojta and M. Mocker. Case formalism for singular normal modes of the Vlasov-BGK equation. *Phys. Letters A*, 31(5):243–244, 1970.
- [19] S. I. Zaki, L. R. Gardner, and T. J. M. Boyd. A finite element code for the simulation of one-dimensional Vlasov plasmas I. theory. *J. Comput. Phys.*, 79(1):184–199, 1988.
- [20] S. I. Zaki, L. R. Gardner, and T. J. M. Boyd. A finite element code for the simulation of one-dimensional Vlasov plasmas II. applications. *J. Comput. Phys.*, 79(1):200–208, 1988.